Spatial Approach to Cardiac Electrical Dynamics: Evaluation of Surrogate Biomarkers of Differences in Drug-Induced Multichannel Block

Pablo Daniel Cruces, [a, b, *] and Pedro David Arini [a, b]

[a] *Instituto de Ingeniería Biomédica, Universidad de Buenos Aires, Buenos Aires, Argentina*

[b] *Instituto Argentino de Matemática Alberto P. Calderón, Consejo Nacional de Investigaciones Científicas y Técnicas, Buenos Aires, Argentina*

Background and Aims. Torsade de Pointes (TdP), a side effect of many marketed drugs, can lead to sudden cardiac death. Regulatory guidelines require quantification of hERG channel block by QT interval prolongation on ECG, although its predictive value remains low. To propose a novel normalization technique for vectorcardiographic loops, enabling improved derivation of conventional and new indices for the robust identification of multiple cardiac ion channel blockades associated with TdP risk.

Methods. A robust method was developed to obtain angular parameters from ECG loops by normalizing for baseline drift using principal component analysis. Linear (via differentiation) and angular (via quaternion algebra) velocities were assessed to identify differential features between multichannel and selective hERG-blocking drugs. Furthermore, bidirectional baseline correction allowed more accurate extraction of ECG wave extrema and peaks, improving the robustness of the QT interval and other temporal measurements. The proposed dynamic biomarkers were evaluated in 22 subjects enrolled in a clinical trial of four known QT-prolonging drugs.

Results. The two high-risk drugs exhibited drug-induced changes ($p < 0.0005$) in velocity during ventricular repolarization. Strong calcium or sodium blockers reduced the effect on velocity caused by hERG potassium channel block. A tendency to symmetry of angular values was observed with high-risk drugs. The alternative temporal indices showed a high correlation ($r > 0.9$) with standard indices. Differences emerged between the T-wave end and the angular velocity marker of ventricular repolarization end.

Conclusion. Spatial analysis of cardiac signals and the new dynamic measures could complement current standards and support safer drug development.

Key Words: Torsade de pointes, Quaternion, Angular velocity, Principal component analysis, Vector cardiogram.

Introduction

Pharmacological treatment is an important therapeutic tool. All drugs must be carefully evaluated prior to marketing to prevent harm. Many drugs currently on the market have been associated with torsade de pointes (TdP), a potentially fatal type of arrhythmia (1,2). TdP is a potentially fatal polymorphic tachyarrhythmia. The regulatory framework for TdP (3) requires a "thorough QTc" study, an electrocardiographic (ECG) measurement of ventricular activity. Current studies identify QT prolongation as a sensitive but non-specific biomarker for TdP (4,5), that is, QT prolongation alone does not necessarily lead to early afterdepolarization (EAD) events that could trigger TdP (6). A positive, thorough QTc study does not imply denial of drug approval, but requires further studies which often lead to unwarranted rejection of the compound due to their cost and risk. The inadequate levels of sensitivity and specificity are often related to reference points in the ECG waves. Therefore, several international organiza-

tions are continuously promoting research for non-invasive complementary biomarkers (7:9).

Some drugs block the human ether-à-go-go-related gene (hERG) potassium channel causing QTc prolongation. These compounds are associated with an increased risk of TdP (1,2). However, sodium and calcium ion fluxes are necessary for the proarrhythmic effect. It has been observed that several drugs that combine blockers of different channels have a lower torsadogenic risk because blocking inward currents prevent EAD (10). Comprehensive in vitro Proarrhythmia Assay (CiPA) initiative has encouraged researchers to incorporate drug effects on multiple ion channels into in silico drug trials to improve TdP risk assessment, since other ion channels may also affect cardiac repolarization and therefore, QTc prolongation is not enough to evaluate cardiac risk (11,12). Some authors have proposed complementary temporal indices such as the time from the onset to the peak (JTp) and the time from the peak to the end (Tpe), both measurements in the T-wave (10,13). Although these indices have shown promising results in differentiating drug-induced hERG block from multichannel block, their calculation still requires an accurate determination of the fiducial points.

On the other hand, digital processing of cardiac spatial dynamics provides complementary information to that observed in the projected planes of the ECG (14,15). We have previously shown a spatial study of TdP risk associated with sotalol administration, a strong hERG blocker, using both in vitro models and human ECG recordings (16,17). Since blockade of different ion channels induces dissimilar alterations in cardiac conduction velocity, the assessment of new biomarkers from the dynamics of cardiac loops could offer a computational tool to differentiate the effects of ion channel blockers. Here, we present a novel method for filtering, segmentation, and normalization of ECG signal loops to enable the robust calculation of velocity biomarkers of the cardiac electrical vector. These biomarkers can not only differentiate multichannel effects but also provide different estimates of ECG wave extrema and peaks, potentially increasing the specificity of state-of-the-art indices. We hope that these ideas will contribute to the development of safe pharmacological therapies using non-invasive techniques.

Materials and Methods

Clinical Study Dataset

The Electrocardiogram Ranolazine, Dofetilide, Verapamil, Quinidine (ECGRDVQ) database includes 12-lead ECG recordings from 22 healthy subjects (26.9 $\pm$ 5.5 years, 50 % female) who participated in a randomized, double-blind, five-period crossover clinical trial. The database was designed to compare the effects of four known QT-prolonging drugs versus placebo: a single dose of 500 μg dofetilide, 400 mg quinidine sulfate, 1500 mg ranolazine, 120 mg verapamil hydrochloride (13,18). Dofetilide and quinidine had similar pharmacokinetic profiles, peaking at 2.5 h; the former is a pure hERG blocker and the last has slightly additional calcium and sodium channel blocking effects. Both are high-risk drugs on the CiPA list (7). Verapamil (peak at 1 h) and ranolazine (peak at 4 h) are potassium blockers with the addition of potent calcium and sodium blockers, respectively (both are low-risk drugs). There was a 7 d washout period between each 24 h treatment period. Three 10 s ECG recordings were obtained in a supine position at each one of the following time-points: :0.5 h (pre-dose), 0.5, 1, 1.5, 2, 2.5, 3, 3.5, 4, 5, 6, 7, 8, 12, 14, and 24 h (post-dose). ECG was recorded at 500 Hz of sampling frequency (Fs) with an amplitude resolution of 2.5 μV with stable heart rates and maximum signal quality. The resulting 5232 ECGs were up-sampled to 1000 Hz. Semi-automated fiducial point annotations are provided in the files.

Preprocessing

The study of the dynamics of cardiac electrical vectors requires a spatial approach. We obtained the orthogonal XYZ leads through the inverse Kors matrix (19). All beats in each 10 s ECG recording were averaged taking the position of the QRS complex ($\hat{R}$) as the reference point. Three signals were then segmented: the QRS complex ($\hat{R}$: 70 ms to $\hat{R}$ + 70 ms), the T-wave (300 ms after QRS) and the P-wave (150 ms before QRS). The exact positions of onset and end of each wave are not necessary, because they are determined with the angular velocity maxima. For each signal, a bidirectional 5th order low-pass Butterworth filter with a cutoff frequency of 10 Hz, 20 Hz and 40 Hz, respectively was applied for noise reduction.

Loop Normalization

Each segmented signal represents a three-dimensional loop. Figure 1 shows an example of a T-wave loop of XYZ leads. This loop has a velocity profile that is strongly affected by zero crossings due to the nonlinearity of the baseline. To avoid these alterations, we developed a normalization algorithm that shifts the loop along its central energy axis in order to separate it from zero. For this purpose, we apply a principal component analysis (PCA) technique. Then, we decompose the loop (L) of three leads and N samples as: $L = [l_x, l_y, l_z] = USV^T$ (1) where $U = [u_1, u_2, u_3]$ is a 3×3 matrix, V is NxN and the singular value matrix S is 3xN. Moving the loop away from the origin gives us two possibilities: to move the loop towards positive values in the first component (u_1) or towards negative ones (Figure 1A and B). In this way, we add the two possible offset values to the loop: $l'_i = l_i + k.u_1 \; \forall i = 1 \ldots N$ (2) and l'_i are the new values of the original XYZ signal after it has

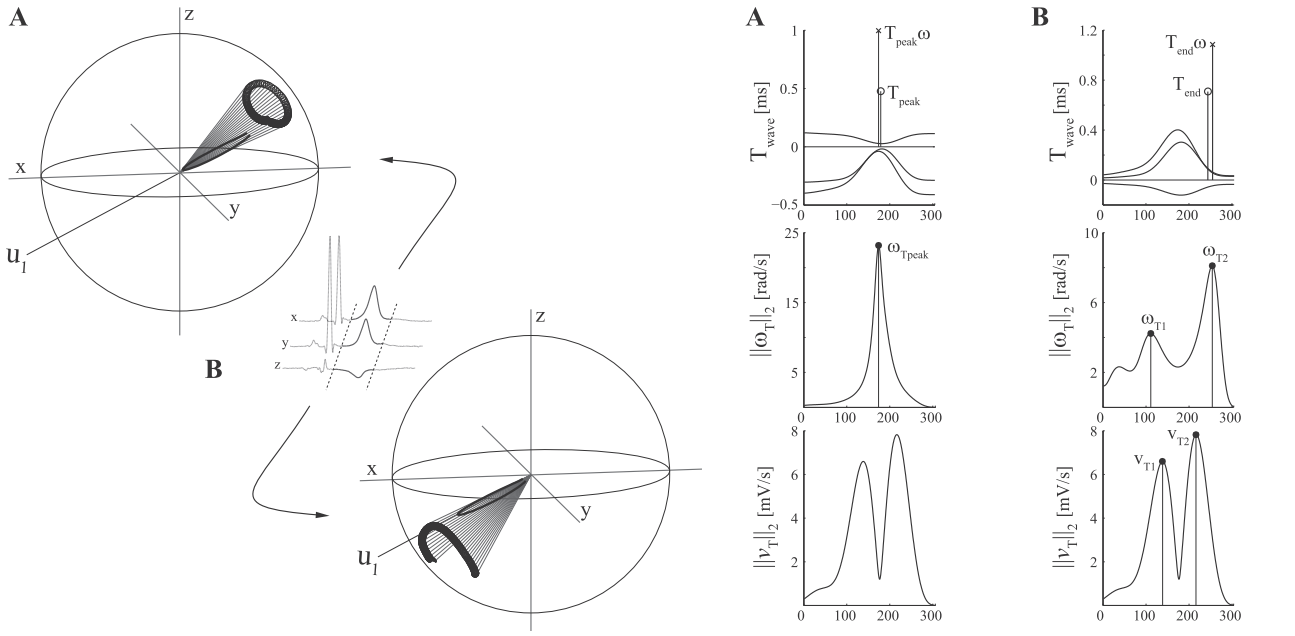

Figure 1. T-wave loop normalization in the three-dimensional space. A. Displacement toward negative values in the principal component (u_1); B. Displacement toward positive values. In each case, the loop is projected onto the sphere of unitary radius. The two-norm angular (ω_T) and linear (v_T) velocity signals and their maximums are also shown. Dataset annotation points are marked with "o"; fiducial points obtained from angular velocity are marked with "x".

been shifted k-times in the principal direction. The value of k in each case is the minimum multiple of the resolution value needed to make the loop positive or negative on axis u_1.

Quaternion Velocity Biomarkers

The linear and angular velocities of each cardiac loop represent fundamental parameters of the vector dynamics and have recently been studied as possible biomarkers of cardiac risk (20,21). Given a sampling frequency F_s, the linear velocity v is obtained directly by numerical differentiation of the spatial signal ($L[n] = [l_x[n], l_y[n], l_z[n]]$) for each nth sample (Eq. 3) and its two-norm is independent of the normalization (Figure 1A, and B). $v[n] = (L[n+1] - L[n]).F_s$ (3).

On the other hand, we obtain the spatial angular velocity from quaternions (22). Quaternions are hypercomplex numbers that are very useful for calculating spatial rotations. This method allows obtaining dynamic features, such as angular velocity, with very low computational uncertainty (23). The loops were normalized to a unitary sphere (Figure 1) and for each nth sample a quaternion $q[n]$ was obtained: $q[n] = (0, L[n])/\|L[n]\|$ (4).

Using numerical differentiation on the sequence of quaternions, $q[n] = (q[n+1] - q[n]).F_s$ (5).

We obtained the angular velocity from the imaginary part of the Poisson formula following the product rule for quaternions (24). The nth quaternion conjugate is denoted as $\underline{q}[n]$: $\omega[n] = q[n] \times \underline{q}[n]$ (6).

Since there are two possible displacement values for the loops, we calculate the two-norm maximum velocity for each. By calculating ω through the loop shifted towards the negative values of the u_1 axis, we obtain the peak (maximum: 'm') of the wave: $\omega_{Lm} = max(\|\omega\|)$. The onset ω_{L1} and end ω_{L2} of the wave are the maxima of ω towards both sides of the ω_{Lm} which are calculated from the loop shifted to the positive values of u_1. As Figure 1 shows, the angular velocity maximums indicate the peak (ω_{Tm}: Figure 1A) and the extremes (ω_{T1} and ω_{T2}: Figure 1B) of the T-wave. These maximums strongly approximate the dataset annotations. Consequently, we obtain not only useful morphology descriptors for the study of ionic conduction changes, but also time signatures of fiducial points. Figure 2 shows an example of the proximity between the Tend time mark and ω_{T2}. These signatures enable us to define variants of standard biomarkers: $QT_{\omega c} = (\omega_{T2} - \omega_{QRS1})/\sqrt{RR}$ (7) where ω_{QRS1} is the first maximum of angular velocity of the QRS complex. $QT_{\omega c}$ represents an alternative measure of QTc, which is the index used in regulatory studies. Here, QTc is the QT corrected by the Bazett's formula (25), i.e., QT divided by the square root of RR interval (reciprocal of heart rate). Furthermore, we define $\{JTp_{\omega c} = (\omega_{Tm} - \omega_{QRS2})/\sqrt{RR}\ Tpe_{\omega c} = (\omega_{T2} - \omega_{Tm})/\sqrt{RR}$ (8) where ω_{QRS2} is the last maximum of angular velocity of the QRS complex. $JTp_{\omega c}$ could be an alternative of JTpc (also corrected by Bazett's formula),

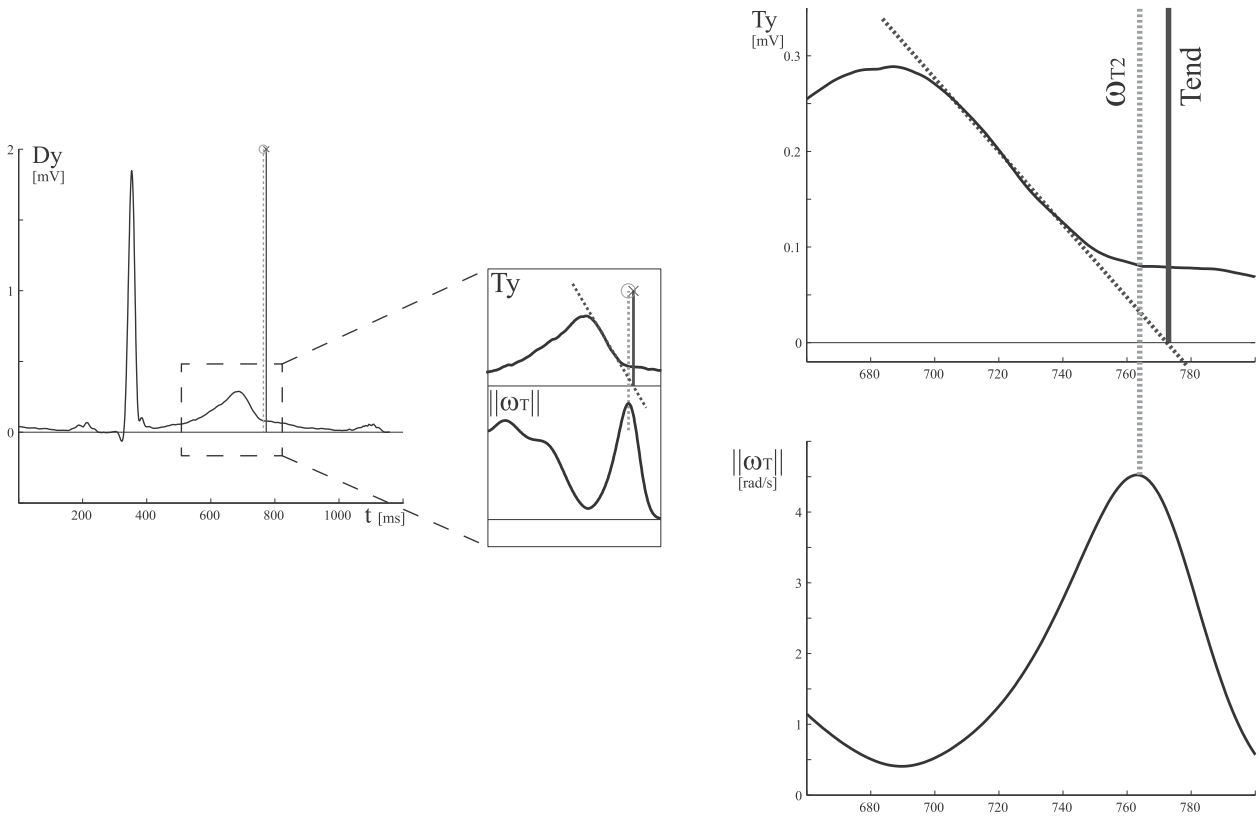

Figure 2. Alternative temporal measurement of the T-wave end obtained from angular velocity, shown as an example on the Dy lead.

which is a measure of early ventricular repolarization duration and a useful biomarker for distinguishing hERG blockers that prolong the QT interval from those that affect multiple ion channel currents (10). Similarly, $Tpe_{\omega c}$ is an alternative to the standard measure of late ventricular repolarization: Tpec.

Finally, we can define the dynamic widths (duration: "d") of the waves from the first and last maximums of angular velocity: $L_{d\omega} = (\omega_{L2} - \omega_{L1})$ (9) where L is any of the QRS, T, or P loops.

Statistical Analysis

Linear and angular velocity maximums are evaluated at each time point for each drug (in the clinical study dataset section). A population assessment was also carried out to confirm that the indices were not affected during placebo administration. A Kolmogorov-Smirnov normality test was performed, followed by a Wilcoxon test to assess significant ($p < 0.05$) changes "Δ" in dynamic signals during drug peak and pre-dose recordings. Additional analysis of the temporal evolution of the dynamic indices was performed using mean estimation with bootstrapping techniques.

Finally, the novel temporal biomarkers $JTp_{\omega c}$, $Tpe_{\omega c}$ and $QT_{\omega c}$ were also evaluated and compared with the standards JTpc, Tpec and QTc via correlation and Bland-Altman plots.

Results

Loop normalization provided clearly marked peaks in the angular signals (Figure 1), which allowed us to define the dynamic indicators and use them to determine wave onsets, peaks, and ends. Table 1 shows the significant drug-induced changes (Δ) that were observed in the dynamic indicators from baseline to the maximum drug plasma concentration. Dofetilide showed the greatest differences in both linear and angular velocities during ventricular repolarization. A reduction in linear velocity was accompanied by an increase in angular velocity during early repolarization. Quinidine also showed similar effects with higher p-values. Strong calcium or sodium blockers would seem to reduce the effect on velocities caused by blocking hERG potassium channels, since ranolazine and verapamil showed more moderate trends. On the other hand, a reduction in the maximum linear velocity of the P wave was observed during the quinidine peak. No significant differences were found in the QRS complex.

The largest changes in velocity occur at the point of the highest drug concentration in the blood. Figure 3A shows dofetilide-induced changes (mean $\pm$ 95 % confidence in-

Table 1. Statistically significant drug-induced changes (Δ) in dynamic indices were observed from pre-dose to drug peak (mean ± SD).

Index	Dofetilide (I_{Kr})	Quinidine (I_{Kr},I_{Na},I_{Ca})	Ranolazine (I_{Kr},I_{Na})	Verapamil (I_{Kr},I_{Ca})
$\Delta\omega_{T1}[\frac{rad}{s}]$	3.90±3.34[c]	4.48±5.25[c]	2.16±2.36[b]	1.51±2.26[a]
$\Delta\omega_{T2}[\frac{rad}{s}]$	−2.40±4.71[a]			
$\Delta v_{T1}[\frac{m\hat{V}}{s}]$	−3.91±1.54[c]	−3.99±1.68[c]		
$\Delta v_{T2}[\frac{m\hat{V}}{s}]$	−4.89±1.89[c]	−5.57±1.96[c]	−2.57±1.31[a]	
$\Delta QT_{\omega c}[ms]$	61.72±19.87[c]	56.81±35.52[c]		
$\Delta JTp_{\omega c}[ms]$	38.77±22.07[c]			
$\Delta Tpe_{\omega c}[ms]$	20.82±31.39[a]	17.44±39.69[a]	6.38±11.72[a]	
$\Delta T_{d\omega}[ms]$	57.71±47.09[c]	34.02±50.84[a]		
$\Delta v_{P2}[ms]$		1.46±1.88[b]		
$\Delta P_{d\omega}[ms]$				15.30±34.80[a]
$\Delta QT_c[ms]$	82.61±25.02[c]	82.27±31.26[c]		
$\Delta JTp_c[ms]$	30.99±18.23[a]			
$\Delta Tpe_c[ms]$	47.74±30.90[c]	49.16±30.67[c]	13.87±8.14[c]	7.62±5.63[a]

The p from the Wilcoxon test is shown as: [a]$p < 0.05$, [b]$p < 0.005$ and [c]$p < 0.0005$. Significant variations in the standard temporal indices are reported at the end of the table.

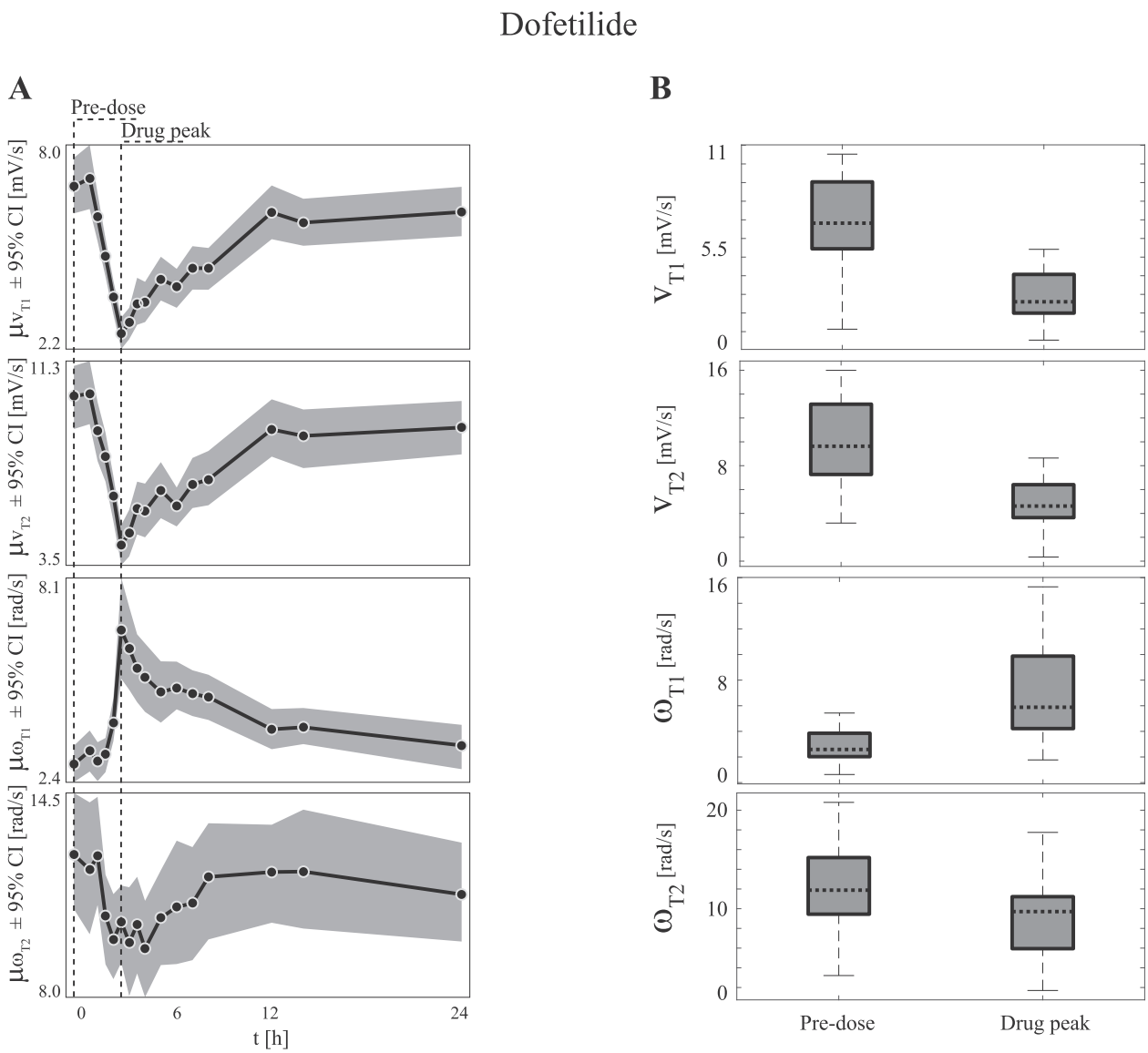

Figure 3. A. Drug-induced velocity changes throughout the 24 h duration of the trial. The mean of the linear and angular velocity maximums in each half of the T-wave are shown; B. Box-and-whisker diagram of velocity variation at dofetilide peak plasma concentration.

terval) from control (pre-dose) to 24 h post-dose. Similarly, a tendency toward symmetry can be observed in the ratio of the velocity maxima. That is, angular velocity had an average ratio of $\frac{\omega_{T2}}{\omega_{T1}} \approx 4.1$ in the baseline signals, and increased in ω_{T1} and decreased in ω_{T2}, reaching an average ratio of $\frac{\omega_{T2}}{\omega_{T1}} \approx 1.4$ during the dofetilide peak. Linear velocity showed a reduction in both halves of the T-wave, exhibiting a ratio of $\frac{v_{T2}}{v_{T1}} \approx 1.5$. Figure 3B shows the box-and- whisker plots of the maximum observed variations, highlighting statistical significance.

Regarding the standard temporal parameters, Tpec showed significant differences across the four drugs. In contrast, QTc and JTpc exhibited significant differences only for the high-risk drugs (Table 1). Their dynamic variants: $QT_{\omega c}$, $JTp_{\omega c}$ and $Tpe_{\omega c}$, showed a high degree of correlation ($r > 0.9$) in the pre-dose signals. However, the T-wave end marker provided in the database was displaced from the ω_{T2} marker in the drug-peak signals. This generates shifts in the Bland-Altman plots of $QT_{\omega c}$ and $Tpe_{\omega c}$, as seen in Figure 4.

Finally, a significant increase in the dynamic width of the T-wave ($T_{d\omega}$) was observed in both high-risk drugs: dofetilide and quinidine. On the other hand, the verapamil peak showed an increase in the dynamic width of the P-wave.

Discussion

Although drug-induced TdP has a low incidence rate, it is gaining recognition as a serious medical problem, resulting in syncope, sudden cardiac arrest or death, or even a misdiagnosis of a seizure disorder (5,26). Torsadogenicity involves the pharmacological blockade of the hERG channel, which produces increases in action potential duration and, consequently, QT interval prolongation. This leads to an increased susceptibility to proarrhythmic events (27). Safety regulatory guidelines require the quantification of hERG channel blockade via QT interval prolongation for all new drugs (3). However, the proarrhythmic effect requires sodium and calcium ion currents, so the addition of calcium and sodium blockers could prevent repolarization failure, i.e., EAD which could trigger TdP (13). Moreover, automated QT interval measurement can be inaccurate, especially when the electrocardiogram baseline is abnormal or noisy (26). A recent study showed the low specificity of the QT interval: out of 2707 cases of QT prolongation, only 10 % wereTdP cases (9). Another study based on the US Food and Drug Administration's Adverse Event Reporting System observed a large number of risk medications that were not included in the CredibleMeds QT interval drug lists (2,28). To address these limitations, the CiPA initiative has proposed to develop novel biomarkers and systematically integrate drug effects on multiple ion channels into in silico clinical trials to improve current TdP risk standards (3,12).

The study of electrocardiography from a spatial perspective has provided promising results in the development of diagnostic indices for malignant arrhythmias (14,17). This study presents a new method that uses a baseline wander normalization on ECG loops to obtain angular parameters. The analysis of the dynamic variables has allowed us to identify differential features of multichannel drugs compared to hERG drugs.

Furthermore, bidirectional baseline correction enabled alternative measurements of the extrema and peaks of ECG waves. This allows the calculation of the QT interval and other temporal indices such as JTpc and Tpec without relying on the current method to identify T-wave onset and end. These standard indices have shown promising results as complementary biomarkers for distinguishing multichannel effects. However, determining the end of the T-wave remains a well-known and complex problem, and continues to be a subject of discussion (29,30). In this sense, the location of the angular velocity maxima allowed us to robustly calculate biomarkers that quantify similar measures. In the control signals (pre-dose), it could be observed that the mark of T-wave end corresponded to the position of ω_{T2} while the J point was regularly positioned 20 ms after ω_{QRS2}. In this condition, our alternative indices presented high correlation and Bland-Altman graphs with good agreement (Figure 4). However, in the signals corresponding to peak in plasma of high-risk drugs (dofetilide and quinidine), a shift was observed in the $QT_{\omega c}$ and $Tpe_{\omega c}$ graphs. In these signals, the linear velocity maxima and the T-wave slopes underwent a significant reduction. Therefore, it is possible that the T-wave end mark in the database, obtained using the standard method (crossing the downward slope of the vector magnitude with the baseline), has additional deviation during this time. After normalization of the loops, a strong deflection in angular velocity can be observed in the second half of the T-wave. This deflection seems to be a more reliable indicator of the end of the T-wave and more accurately represents the actual end of ventricular repolarization. While the results are promising, further studies are required to better understand the sources of the observed differences and their potential to improve the specificity of the indices in the current guidelines. Moreover, alternative correction formulas for temporal intervals may be necessary in addition to the Bazett formula when heart rates are unusually high or low.

The dynamic features, which are complementary to the standard temporal measures, showed greater changes with high-risk drugs. Regarding the maximum angular velocity, dofetilide showed a significant decrease in ω_{T2} (Table 1). Together with the increase in ω_{T1}, this tendency approached symmetry of angular values. These values were reached at the time of the drug peak (Figure 3). Previous studies have suggested that repolarization symmetry, as measured by areas and velocities, is a risk marker

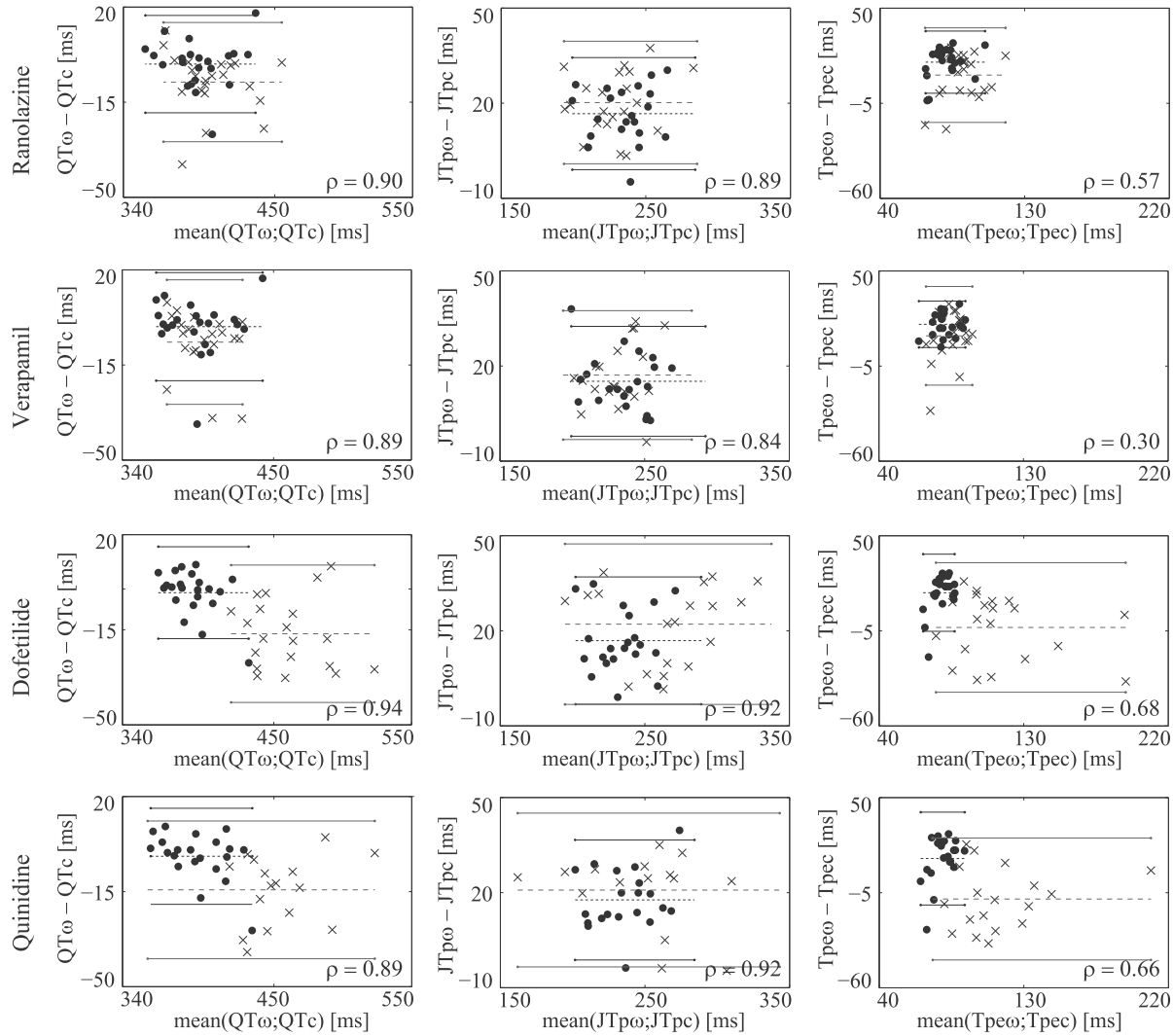

Figure 4. Bland-Altman plots for the comparison of the standard temporal biomarkers: QTc, Tpec and JTpc, as well as their dynamic variants: $QT_{\omega c}$, $Tpe_{\omega c}$ and $JTp_{\omega c}$. The corresponding difference bias between the two measurements is shown with a dashed line and the 95 % limits of agreement are shown with a solid line. "•" are pre-dosing values and "x" are drug peak values, respectively.

for arrhythmias (17,31,32). However, this symmetry may be limited to spatial parameters, since some authors have suggested a slight tendency toward temporal asymmetry when considering the relationship between early and late repolarization times (18). ω_{T1} also increased significantly with quinidine. Low-risk drugs showed smaller increases in maximum angular velocity during the initial half of the T-wave. Regarding linear velocities, neither ranolazine nor verapamil showed significant changes in v_{T1} or v_{T2}.

The dynamic width of the T-wave ($T_{d\omega}$), obtained using angular velocity, increased significantly with dofetilide, which also presented the largest increases in JTpc and Tpec. These results are consistent with others showing equal prolongation of early and late repolarization (13).

Finally, dynamic changes in the P-wave were observed only in quinidine and verapamil (Table 1). These changes may be due to an altered conductive response of the atrioventricular node, which is regulated by calcium channels (13). The P-wave dynamic width was significantly prolonged with verapamil but not with quinidine, which showed increases in downslope velocity.

Conclusion

The new dynamic measures obtained through quaternions after normalization of the ECG loops have shown robustness when evaluated with different drugs. Moreover, a novel method for measuring the standard drug regulatory

parameters was presented with promising results. These biomarkers could complement current standards and contribute significantly to the development of safe pharmacological therapies.

Conflicts of Interest

The authors declare that there are no conflicts of interest.

Acknowledgments

This work was supported by CONICET, under project PIP #112–20130100552CO, and by the MINCYT Agency, under project PICT 2145–2016, Argentina.

References

1. Camm A. Hopes and disappointments with antiarrhythmic drugs. International Journal of Cardiology 2017;237:71–74. doi:10.1016/j.ijcard.2017.03.056.
2. CredibleMeds. QT drug lists. https://www.crediblemeds.org. (Accessed July 10, 2024).
3. Strauss D, Wu W, Li Z, et al. Translational models and tools to reduce clinical trials and improve regulatory decision making for QTc and proarrhythmia risk (ICH E14/S7B updates). Clinical Pharmacology & Therapeutics 2021;109:319–333. doi:10.1002/cpt.2137.
4. Krumpholz L, Wiśniowska B, Polak S. Open-access database of literature derived drug-related torsade de pointes cases. BMC Pharmacology and Toxicology 2022;23:11. doi:10.1186/s40360-021-00548-0.
5. Woosley R. Drug-induced torsades de pointes. In: Tislade JE, editor. Torsades De Pointes. Elsevier Inc; 2022. p. 39–50. doi:10.1016/B978-0-12-821446-6.00007-9.
6. Zhao P, Li P. Transmural and rate-dependent profiling of drug-induced arrhythmogenic risks through in silico simulations of multichannel pharmacology. Scientific Reports 2019;9:18504. doi:10.1038/s41598-019-55032-x.
7. Colatsky T, Fermini B, Gintant G, et al. The comprehensive in vitro proarrhythmia assay (CIPA) initiative - update on progress. Journal of Pharmacological and Toxicological Methods 2016;81:15–20. doi:10.1016/j.vascn.2016.06.002.
8. Strauss DG, Gintant G, Li Z, et al. Comprehensive in vitro proarrhythmia assay (CIPA) update from a cardiac safety research consortium /health and environmental sciences institute / FDA meeting. Therapeutic Innovation & Regulatory Science 2018;53:519–525. doi:10.1177/2168479018795117.
9. Uchikawa M, Hashiguchi M, Shiga T. Drug-induced QT prolongation and torsade de pointes in spontaneous adverse event reporting: a retrospective analysis using the japanese adverse drug event report database (2004:2021). Drugs Real World Outcomes 2022;9:551–559. doi:10.1007/s40801-022-00328-0.
10. Hnatkova K, Vicente J, Johannesen L, et al. Heart rate correction of the J-to-tpeak interval. Scientific Reports 2019;9:15060. doi:10.1038/s41598-019-51491-4.
11. Woosley R, Romero K, Heise C, et al. Adverse drug event causality analysis (ADECA): a process for evaluating evidence and assigning drugs to risk categories for sudden death. Drug Safety 2017;40:465–474. doi:10.1007/s40264-017-0519-0.
12. Zhou X, Qu Y, Passini E, et al. Blinded in silico drug trial reveals the minimum set of ion channels for torsades de pointes risk assessment. Frontiers in Pharmacology 2020;10:1643. doi:10.3389/fphar.2019.01643.
13. Johannesen L, Vicente J, Mason J, et al. Differentiating drug-induced multichannel block on the electrocardiogram: randomized study of dofetilide, quinidine, ranolazine, and verapamil. Clinical Pharmacology & Therapeutics 2014;96:549–558. doi:10.1038/clpt.2014.155.
14. Vondrak J, Penhaker M. Review of processing pathological vectorcardiographic records for the detection of heart disease. Frontiers in Physiology 2022;13:856590. doi:10.3389/fphys.2022.856590.
15. Cruces P, Arini P. Quaternion-based study of angular velocity of the cardiac vector during myocardial ischaemia. International Journal of Cardiology 2017;248:57–63. doi:10.1016/j.ijcard.2017.06.095.
16. Cruces P, Torkar D, Arini P. Dynamic features of cardiac vector as alternative markers of drug-induced spatial dispersion. Journal of Pharmacological and Toxicological Methods 2020;104:106894. doi:10.1016/j.vascn.2020.106894.
17. Cruces P, Toscano A, Rodriguez A, et al. Drug-induced symmetry effects on ventricular repolarization dynamics. Biomedical Signal Processing and Control 2022;81:104493. doi:10.1016/j.bspc.2022.104493.
18. Vicente J, Johannesen L, Mason J, et al. Comprehensive t wave morphology assessment in a randomized clinical study of dofetilide, quinidine, ranolazine, and verapamil. Journal of the American Heart Association 2015;4:001615. doi:10.1161/JAHA.114.001615.
19. Kors JA, Van Herpen G, Van Bemmel JH. Reconstruction of the Frank vectorcardiogram from standard electrocardiographic leads: diagnostic comparison of different methods. European Heart Journal 1990;11:1083–1092. doi:10.1093/oxfordjournals.eurheartj.a059647.
20. Cruces P, Arini P. A novel method for cardiac vector velocity measurement: evaluation in myocardial infarction. Biomedical Signal Processing and Control 2016;28:58–62. doi:10.1016/j.bspc.2016.04.003.
21. Starc V, Schlegel T. Delineation of QRS offset by instantaneous changes in ECG vector angle can improve detection of acute inferior myocardial infarctions. Journal of Electrocardiology 2016;49:337–344. doi:10.1016/j.jelectrocard.2016.02.019.
22. Cruces P, Llamedo Soria M, Arini P. Velocity tracking of cardiac vector loops to identify signs of stress-induced ischaemia. Medical and Biological Engineering and Computing 2022;60:1313–1321. doi:10.1007/s11517-022-02503-5.
23. Goldman R. Rethinking Quaternions: Theory and Computation. California: Morgan & Claypool; 2010.
24. Poznyak A. Modelado Matemático de Los Sistemas Mecánicos, Eléctricos y Electromecanicos. Ciudad de México: Pearson Educación; 2005.
25. Yap Y, Camm A. Drug induced QT prolongation and torsades de pointes. Heart 2003;89:1363–1372. doi:10.1136/heart.89.11.1363.
26. Davies R, Beausejour Ladouceur V, Green M, et al. The 2023 Canadian cardiovascular society clinical practice update on management of the patient with a prolonged QT interval. Canadian Journal of Cardiology 2023;39:1285–1301. doi:10.1016/j.cjca.2023.06.011.
27. Iseppe A, Ni H, Zhu S, et al. Sex-specific classification of drug-induced torsade de pointes susceptibility using cardiac simulations and machine learning. Clinical Pharmacology & Therapeutics 2021;110:380–391. doi:10.1002/cpt.2240.
28. Wu Z, Zhou P, He N, et al. Drug-induced torsades de pointes: disproportionality analysis of the united states food and drug administration adverse event reporting system. Frontiers in Cardiovascular Medicine 2022;9:966331. doi:10.3389/fcvm.2022.966331.
29. Malik M, Huikuri H, Lombardi F, et al. Is the Tpeak-Tend interval as a measure of repolarization heterogeneity dead or just seriously wounded? Heart Rhythm 2019;16:952–953. doi:10.1016/j.hrthm.2019.01.015.
30. Antzelevitch C, Di Diego J. Counterpoint tpeak-tend interval as a marker of arrhythmic risk. Heart Rhythm 2019;16:954–955. doi:10.1016/j.hrthm.2019.01.017.
31. Andersen M, Xue J, Graff C, et al. New descriptors of T-wave morphology are independent of heart rate. Journal of Electrocardiology 2008;41:557–561. doi:10.1016/j.jelectrocard.2008.07.021.
32. Di Bernardo D, Murray A. Explaining the T-wave shape in the ECG. Nature 2000;403:40. doi:10.1038/47409.